Photoconductive detection of hydrogen in ZnO and rutile TiO2

E. V. Lavrov, T. Mchedlidze, and F. Herklotz

Articles you may be interested in

A strategy to stabilise the local structure of Ti4+ and Zn2+ species against aging in TiO2/aluminium-doped ZnO bi-layers for applications in hybrid solar cells
J. Appl. Phys. **116**, 054907 (2014); 10.1063/1.4892039

Continuous wave ultraviolet-laser sintering of ZnO and TiO2 nanoparticle thin films at low laser powers
J. Appl. Phys. **113**, 044310 (2013); 10.1063/1.4788906

Photoconductivity and trap-related decay in porous TiO2/ZnO nanocomposites
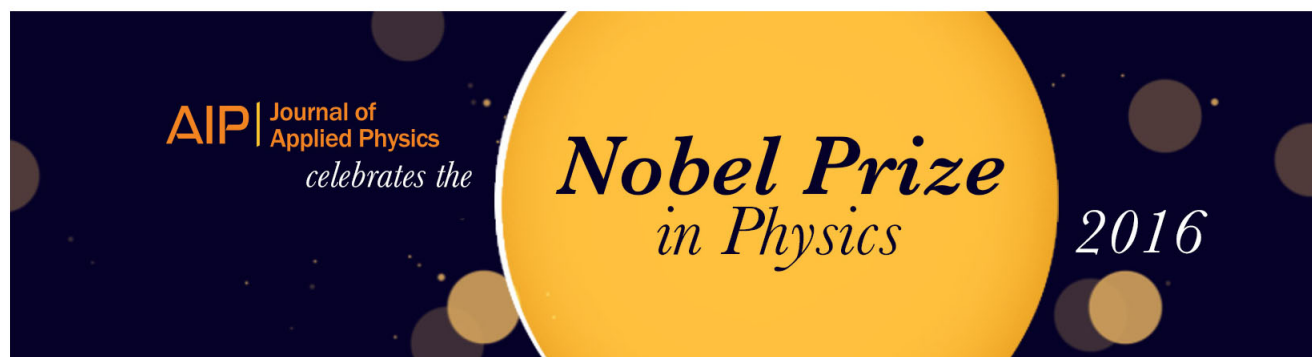J. Appl. Phys. **110**, 123513 (2011); 10.1063/1.3662954

Infrared absorption spectroscopy on OH–Ni complex in hydrothermally grown ZnO
J. Appl. Phys. **105**, 093516 (2009); 10.1063/1.3116721

Doping of spray-pyrolyzed ZnO thin films through direct diffusion of indium: Structural optical and electrical studies
J. Appl. Phys. **98**, 023509 (2005); 10.1063/1.1985967

Photoconductive detection of hydrogen in ZnO and rutile TiO$_2$

E. V. Lavrov,[1,a)] T. Mchedlidze,[1] and F. Herklotz[2]
[1]*Technische Universität Dresden, 01062 Dresden, Germany*
[2]*Freie Universität Berlin, 14195 Berlin, Germany*

Hydrogen donors in ZnO and rutile TiO$_2$ are probed by means of photoconductivity and IR absorption. It is shown that the O–H bonds giving rise to the local vibrational modes (LVMs) of interstitial hydrogen at 3611 and 3290 cm^{-1} in the case of ZnO and TiO$_2$, respectively, also occur in the photoconductivity spectra as Fano resonances. The effects of isotope substitution, concentration, sample thickness, influence of other donors present in both oxides are considered. Based on the shape and frequency of these resonances, it is concluded that the apparent ionization energy of interstitial hydrogen in rutile TiO$_2$ is less than 300 meV. By a direct comparison, we also demonstrate that photoconductive detection of LVMs of defects in thin semiconductor films is superior to the standard IR absorption. *Published by AIP Publishing.* [http://dx.doi.org/10.1063/1.4960132]

I. INTRODUCTION

Local vibrational mode (LVM) spectroscopy is a versatile tool that provides a wealth of information about the chemistry and symmetry of light defects in the host lattice. The identification of the species is obtained from isotope substitutions, uniaxial stress experiments provide the symmetry, and a thermal treatment gives binding energies. LVM detection by Fourier-transformed IR absorption spectroscopy has been developed as the most versatile technique for defect studies.[1] The theoretical description of defects in solids has advanced lately and allows the calculations of LVMs to a very high precision. Hence, predictions of defect properties can be, in principle, easily verified by means of vibrational spectroscopy.

From the experimental point of view, however, investigation of LVMs of defects in solids is not always an easy task. The situation is simple if vibrational motion of species is decoupled from the lattice phonons and/or electronic excitations. Typically, but not always, this is the case for light impurities such as hydrogen, whose vibrational frequencies are well above most of the elementary excitations in semiconductors.[2]

Situation changes if masses of the vibrating atoms come closer to those of the host lattice. In this case, LVM frequencies occur in strongly absorbing spectral regions of crystals resulting from two-phonon or/and electronic absorption, which makes direct IR absorption experiments practically impossible. The sensitivity of Raman scattering is too low to replace IR absorption in most cases, which seriously restricts the number of direct experimental techniques capable of probing LVMs of defects in semiconductors and hinders the progress in understanding their properties.

Another drawback of IR absorption spectroscopy is the difficulty in determining the electrical activity of the defects since frequencies of vibrational modes are rather insensitive to the charge states of the defect complexes.

Recently, a method of photoconductive detection of LVMs has been proposed to overcome the challenges faced by IR absorption in ionic crystals.[3] The method was successfully applied to investigate hydrogen substituting for oxygen (H$_O$) in ZnO. The calculated LVMs of this complex were found at 760(50) cm^{-1},[4] which is very close to the Reststrahlen band of this material what made IR absorption and thus direct verification of the theoretical predictions practically impossible.

Another advantage of photoconductive detection of LVMs as compared to the absorption spectroscopy is its exceptional sensitivity.[5] A key prerequisite for successful employment of photoconductivity, however, is low-noise ohmic contacts working at helium temperatures.

The principle of the method is shown in Fig. 1. A photocurrent is detected when an incoming photon excites an electron from the ground state of a donor into the conduction
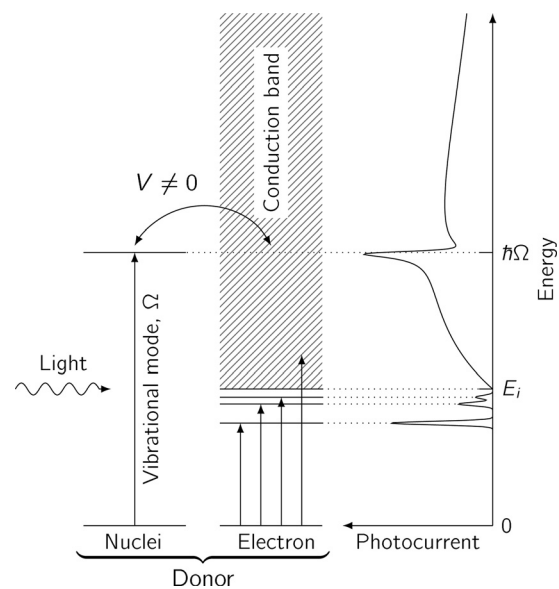

FIG. 1. Schematic view of a photoconductivity spectrum of a shallow donor including a Fano resonance ($q < 0$) due to the vibrational motion (frequency Ω) of its nuclei.

a)edward.lavrov@physik.tu-dresden.de

band of a semiconductor. Alternatively, a photon with the same energy can excite a LVM of the defect. If the two types of excitations are decoupled ($V = 0$), the LVM will result in a *dip* in the broad photoconductivity (PC) spectrum. Note that the sharp lines in the spectrum corresponding to the intrinsic states of an electron are results of the simultaneous or consecutive absorption of a photon and one or more phonons. This mechanism is known as photothermal-ionization.[5]

Another possibility arises if both LVM and electronic excitations originate from the same defect ($V \neq 0$). In this case, the PC spectrum is modified resulting in a *Fano resonance*, the shape of which is given by[6]

$$I(\epsilon) \propto \frac{(q + \epsilon)^2}{1 + \epsilon^2}, \quad \epsilon = \frac{\omega - \Omega_0 - \Delta\Omega}{\Gamma/2}, \quad (1)$$

where Ω_0 is the LVM frequency, Γ is the spectral width of the interacting discrete vibrational state, $\Delta\Omega$ is the additional shift, and q is the line shape parameter. Qualitatively, the shape of the resonance depends on the parameter q. For $q = 0$ the LVM will appear as an anti-resonance, whereas for $q \rightarrow \pm\infty$ it will have a Lorentzian shape. Obviously, the cases of anti-resonance and decoupled vibrational motion ($V = 0$) are difficult to distinguish experimentally, whereas an enhancement of the photocurrent at $\omega \approx \omega_0$ ($q \rightarrow \pm\infty$) will unambiguously imply that this defect is a dominant donor/acceptor in the sample and will therefore unveil the type of its electrical activity.

Here, we report the results of a detailed photoconductivity study aimed at the vibrational motion of hydrogen-related donors in ZnO and rutile TiO$_2$ (preliminary results were reported in Ref. 7). Specifically, the effects of isotope substitution, concentration, sample thickness, and influence of other donors present in the material are addressed.

II. EXPERIMENTAL DETAILS

The photoconductivity and IR absorption measurements were performed with a Bomem DA3.01 Fourier spectrometer equipped with a globar light source and a KBr or CaF$_2$ beamsplitter. The samples were positioned in an exchange-gas cryostat equipped with ZnSe windows. The frequency range 500–5000 cm^{-1} could be covered. The spectral resolution was 0.25–1.0 cm^{-1}. The temperature of the samples was stabilized within 0.4 K in the range of 7–12 K.[8,9]

The nominally undoped ZnO samples used in this work were grown from the vapor phase at the Institute for Applied Physics, University of Erlangen, Germany.[10] The rutile TiO$_2$ samples were commercial (110)-oriented wafers purchased from CrysTec GmbH (Germany) grown by the Verneuil technique with a resistivity above 10 MΩ cm at room temperature.

Hydrogen or/and deuterium were introduced into the samples via thermal treatments in sealed quartz ampules, filled with H$_2$, D$_2$, or H$_2$ + D$_2$ gas (a pressure of 0.5 bar at room temperature). The treatments were performed at 450–800 °C within 1–6 h and were terminated by quenching to room temperature in water. To produce ohmic contacts, the samples were first etched with orthophosphoric acid

(ZnO) or KOH (TiO$_2$) for 1 min at room temperature. Afterwards, two contacts with an area of approximately 2×2 mm^2 were generated by scratching an In-Ga eutectic onto the sample surface.

III. RESULTS AND DISCUSSION

A. ZnO

1. Isotope substitution

To get insight into the advantages and disadvantages of the method of photoconductive detection of local vibrational modes, we consider first interstitial hydrogen in ZnO (H$_{BC}$)—a defect whose properties are very well known.[8,11,12] Here, the hydrogen atom is positioned between the neighboring zinc and oxygen atoms forming an O–H bond aligned parallel to the c axis of the crystal which is characterized by a local vibrational mode with a frequency of 3611 cm^{-1}.[8] Upon replacement with deuterium, the LVM of the defect red-shifts by around a factor of $\sqrt{2}$ down to 2668 cm^{-1}.

Interstitial hydrogen in ZnO is a shallow donor with an ionization energy of 53 meV.[12] Spectroscopic features of H$_{BC}$ were documented in IR absorption, photoluminescence, and Raman scattering. Intrinsic $1s \rightarrow 2p_z(p_{xy})$ donor transitions at around 330 cm^{-1} were also detected in photoconductivity spectra of hydrogenated ZnO samples. Concentration of H$_{BC}$ can be obtained from the intensity of the 3611-cm^{-1} line in the IR absorption spectra.[12] For the treatment performed at 750 °C, it equals approximately 3×10^{17} cm^{-3} what matches the solubility limit of hydrogen at this temperature.[13]

Figure 2 presents sections of photoconductivity spectra taken on ZnO samples treated in H$_2$ (top), D$_2$ (mid), and H$_2$ + D$_2$ (bottom) gas at 750 °C. These spectra reveal that
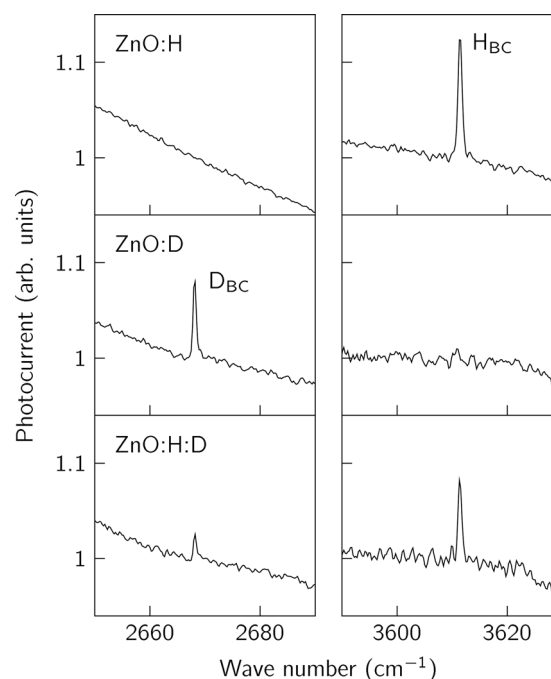
FIG. 2. Sections of photoconductivity spectra taken at $T \leq 10$ K on vapor phase grown ZnO samples treated at 750 °C for 1 h in H$_2$ (top), D$_2$ (mid), and H$_2$ + D$_2$ (bottom) gas.
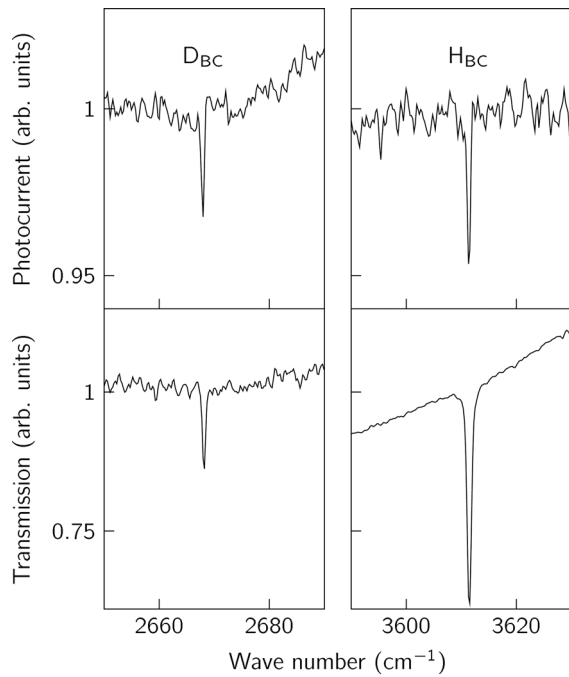
FIG. 3. Sections of photoconductivity (top) and IR transmission (bottom) spectra taken at $T \leq 10$ K on vapor phase grown ZnO sample treated at 800 °C for 1 h in $H_2 + D_2$ gas.
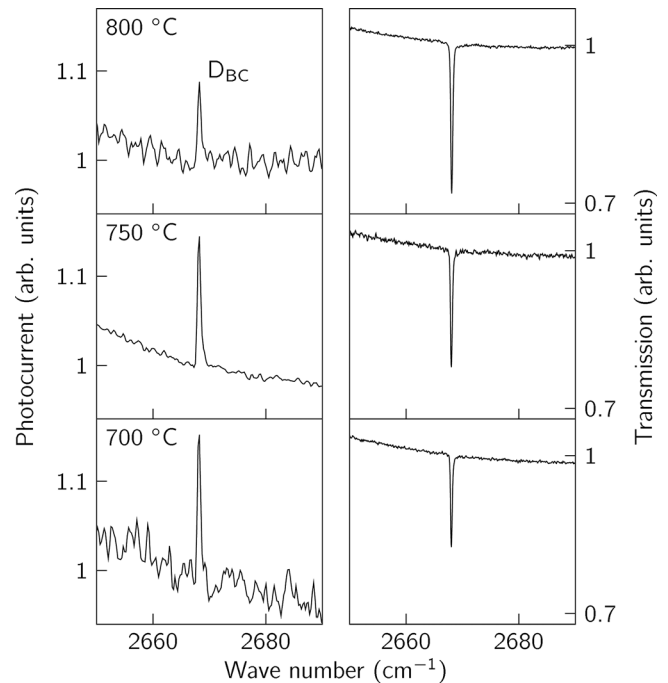

FIG. 4. Sections of photoconductivity (left) and IR transmission (right) spectra taken at $T \leq 10$ K on vapor phase grown ZnO sample treated for 1 h in D_2 gas at 800 (top), 750 (mid), and 700 °C (bottom).

LVM of interstitial hydrogen in ZnO can also be probed by means of photoconductivity. Importantly, photocurrent *enhances* at the frequencies of LVMs due to both H_{BC} and D_{BC} compared to the background current what unambiguously identifies these features as Fano resonances with the parameter $q \to +\infty$ (see Eq. (1)).

The assignment of the defect giving rise to the LVM at $3611 \, \text{cm}^{-1}$ to the hydrogen shallow donor was made on the basis of combined spectroscopic studies including IR absorption, Raman scattering, and photoluminescence measurements.[12] The photocurrent spectra presented in Fig. 2 lead us to the conclusion that a clue about the electrical activity of isolated hydrogen in ZnO could be obtained at much lower cost simply by recording photoconductivity spectra in the region typical for the LVMs of the defect.

The assignment of defects to shallow donors on the basis of the LVM resonances occurring in photocurrent should be done, however, with some care since the shape of these features depends on its amount relative to other electrically active defects available in a sample.

The best way to see this is in the case that both hydrogen isotopes are present in the sample. Here, the LVM of H_{BC} is decoupled ($V = 0$, see Fig. 1) from the electronic transitions of D_{BC} and vise versa. This implies that the resulting signal at around 3611 (2668) cm^{-1} is a combination of the photocurrent of the H_{BC} (D_{BC}) donors with a *positive* peak due to Fano resonances with $q \to +\infty$ and the photocurrent generated by D_{BC} (H_{BC}) donors with a *dip* due to absorption at H_{BC} (D_{BC}). The outcome is therefore a function of the ratio between the two isotopes.

The bottom spectrum shown in Fig. 2 was obtained for the $N_{H_{BC}} : N_{D_{BC}}$ ratio of about 3:2, which was determined

from the IR absorption peaks due to interstitial hydrogen and deuterium.[12] Here, intensities of the Fano resonances due to H_{BC} and D_{BC} are significantly reduced compared to the cases where only one isotope is present in the sample. Figure 3 presents photoconductivity (top) and IR transmission (bottom) spectra of a ZnO sample where the ratio $N_{H_{BC}} : N_{D_{BC}}$ turned out to be 5:2. Here, both LVMs occur as dips in the photoconductivity spectra. We conclude from here that in order to get insight into the "true" shape of the Fano resonance, the donor of interest should dominate the sample.

2. Concentration dependence

Figure 4 shows sections of photoconductivity and IR transmission spectra taken on a ZnO sample treated in D_2 gas at 800 (top), 750 (mid), and 700 °C (bottom). Similar results were obtained for the samples treated with hydrogen. Due to the somewhat better signal-to-noise ratio only the spectra recorded for the deuterium-treated ZnO are presented.

The solubility limit of hydrogen/deuterium strongly depends on a treatment conditions and enhances by approximately a factor of 2 if the temperature raises from 700 to 800 °C.[13] This can be seen from the transmission spectra given in the right panels of the figure. On the other hand, photoconductivity spectra of the same samples presented in the left panels of the figure indicate that the intensity of the Fano resonance due to D_{BC} relative to the background signal is not proportional to the concentration of these donors. Such a behavior should be expected since contrary to IR absorption, the Fano resonance and the background photocurrent have the *same* origin. We explain the reduction of the Fano peak in the PC spectrum taken after the treatment at 800 °C
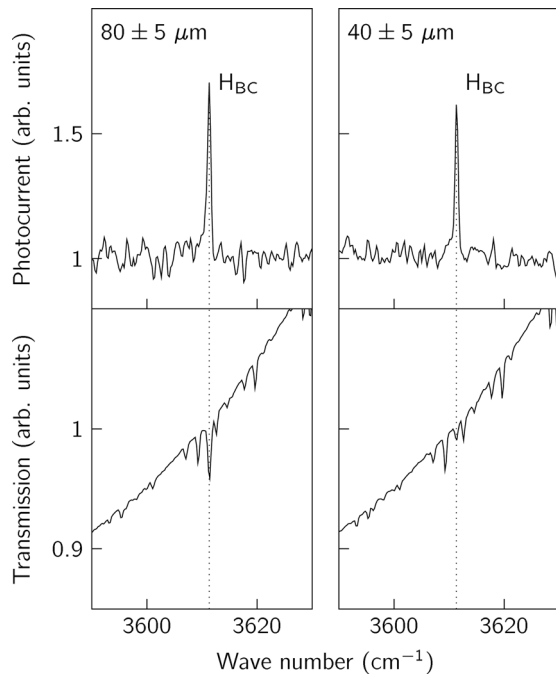
FIG. 5. Sections of photoconductivity (top) and IR transmission (bottom) spectra taken at $T \approx 11$ K on a ZnO sample treated for 1 h in H_2 gas at 750 °C. Sample thickness is 80 ± 5 μm (left) and 40 ± 5 μm (right).
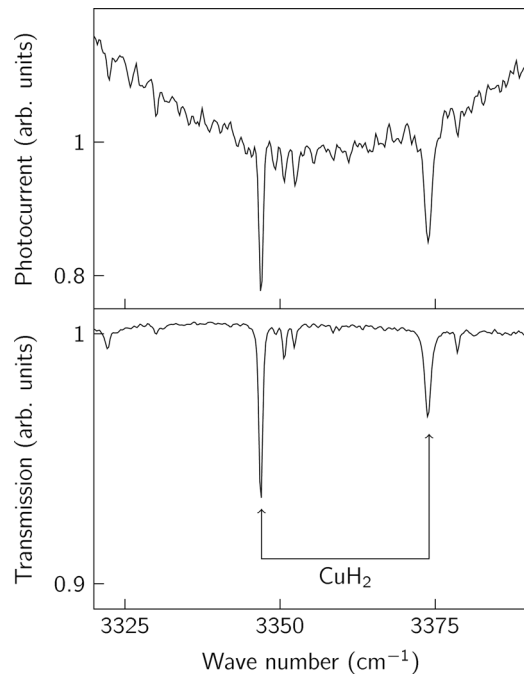

FIG. 6. Sections of photoconductivity (top) and IR transmission (bottom) spectra taken at $T \leq 10$ K on a ZnO sample where the dominant donor is substitutional Al.

by the formation of other vacancy-like donors, for example, D_O, which also takes place at elevated temperatures as ZnO decomposes. The effect of such a formation should be similar to the one discussed above for the samples treated with both H and D isotopes.

3. Sample thickness

An important advantage of the photoelectric spectroscopy method compared with the absorption techniques is the possibility of using the former at very low impurity concentrations since in contrast to the optical absorption, the photoelectric signal does not decrease (within certain limits) with decreasing impurity concentrations.[5] It follows from here that photoelectric method of detection of LVMs of defects can be successfully applied for thin films.

Figure 5 shows sections of photoconductivity (top) and IR transmission (bottom) spectra of a ZnO sample hydrogenated at 750 °C for 1 h. Left spectra were obtained as the sample thickness was 80 ± 5 μm, whereas the spectra in the right panels of the figure were recorded after thinning it down to 40 ± 5 μm via etching in orthophosphoric acid at room temperature. Sharp lines seen in the transmission spectra are due to the residual water vapor in the spectrometer.

It is obvious from the figure that the amplitude of the Fano peak due to the vibrational mode of bond-centered hydrogen does not change significantly as the thickness of the sample goes down to 40 μm. On the other hand, LVM of H_{BC} is hardly seen in the transmission spectrum. Fragility of ZnO has prevented us from thinning the sample further on. Experiments on photoelectric spectroscopy are on the way in order to test the limits of this method and to get insight into the properties of semiconductor thin films grown on different substrates.

4. Other defects

From the description of the method (see Fig. 1), it is clear that photoconductive detection of local vibrational modes is not restricted by electrically active defects. Figure 6 shows sections of photoconductivity (top) and IR transmission (bottom) spectra obtained for a ZnO sample where the dominant donor is substitutional Al rather than interstitial hydrogen. The two dominant lines at 3347 and 3374 cm^{-1} clearly seen in both spectra are due to the local vibrational modes of a defect associated with a copper-dihydrogen complex CuH_2.[14,15] Interestingly, for both 3347 and 3374-cm^{-1} LVMs the drop in the intensity relative to the background is much stronger in the case of photoconductivity than that of the IR transmission.

Theory predicts that CuH_2 acts as a shallow donor in ZnO.[16] One may expect, therefore, that Fano resonances due to the LVMs of this defect have a similar shape to those of H_{BC}, i.e., with $q \rightarrow +\infty$. On the other hand, copper-dihydrogen complex is not the dominant donor in this sample what probably affects the shape of these signals and does not allow to confirm or rule out the conclusions of theory concerning electrical activity of CuH_2.

B. Rutile TiO₂

Interstitial hydrogen in wide band gap oxides typically acts either as an amphoteric impurity or as a donor.[11,17–19] The latter is the case in two most common polymorphs of TiO$_2$, rutile and anatase. The structure of donors in these two types of TiO$_2$ is, however, different revealing differences between anatase and rutile in electrical, magnetic, and optical properties.[20–22] Theory finds that electrons in rutile can localize at a lattice Ti atom, forming a small polaron, which
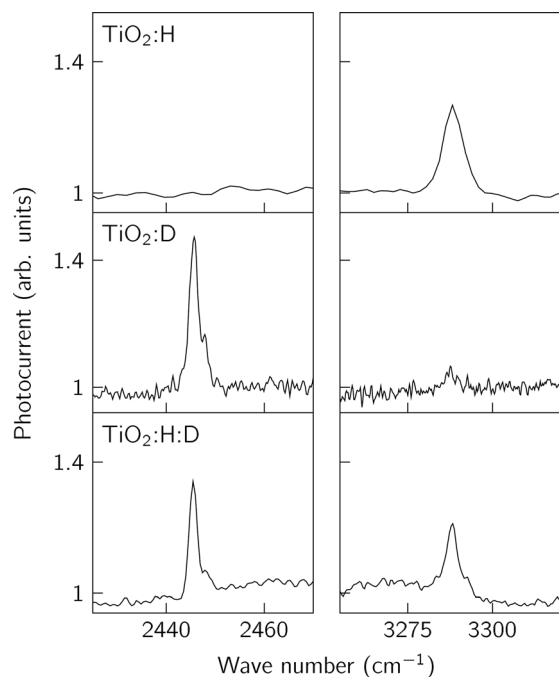
FIG. 7. Sections of photoconductivity spectra taken at $T \approx 7$ K on rutile TiO$_2$ samples treated in the temperature range of 450–520 °C for 1 h in H$_2$ (top), D$_2$ (mid), and H$_2$ + D$_2$ (bottom) gas.
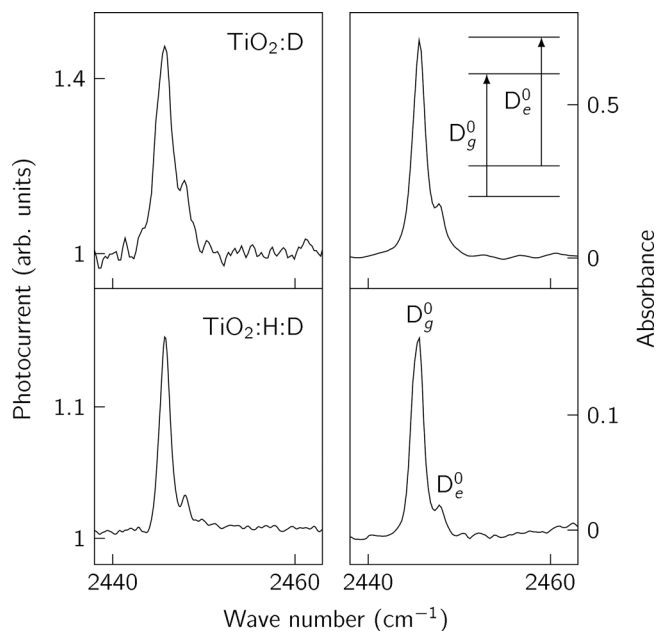

FIG. 8. Sections of photoconductivity (left) and IR absorption (right) spectra taken at $T \approx 7$ K on rutile TiO$_2$ samples treated in the temperature range of 450–520 °C for 1 h in D$_2$ (top) and H$_2$ + D$_2$ (bottom) gas.

hops to neighboring lattice sites, whereas in anatase electrons prefer a delocalized state.[23–25] The latest IR absorption studies on anatase TiO$_2$ match the conclusions of theory.[26,27]

Hydrogen in rutile TiO$_2$ forms a single dative bond to oxygen and is located in the empty c channel of the crystal.[28–30] Some muon spin rotation (μSR) investigations provide an ionization energy of 5–20 meV for isolated hydrogen donor in rutile.[17,31] Other μSR, EPR, and IR absorption studies are in line with the conclusions of theory that the electron associated with the neutral hydrogen center in rutile TiO$_2$ is localized on a nearby Ti atom as a small polaron rather than being delocalized as would be expected for a shallow effective-mass-theory donor.[32–37]

Here, we address the issue of the electrical activity of hydrogen in rutile TiO$_2$ by means of photoconductivity. Figure 7 shows sections of photoconductivity spectra taken on rutile TiO$_2$ samples treated in H$_2$ (top), D$_2$ (mid), and H$_2$ + D$_2$ (bottom) gas in the temperature range of 450–520 °C. The treatments give rise to the features with the frequencies corresponding to the LVMs of interstitial hydrogen and deuterium at around 3290 and 2445 cm^{-1}, respectively.

It was recently shown that the LVM of hydrogen in rutile consists of at least three modes which were assigned to the positive (one) and the neutral (two) charge states of the defect.[9] The modes due to the neutral charge state of the donor were associated with the ground and excited states of hydrogen in the c-channel of rutile. The intensity ratio between the two charge states was found to be temperature-dependent, whereby the full ionization took place at already 60 K. Based on this, it was concluded that isolated hydrogen in rutile acts as a shallow donor.

After replacement of hydrogen with deuterium, the LVMs of the ionized (D$^+$) and the two neutral (D$_g^0$ and D$_e^0$)

charge states were found to have frequencies at 2445.0, 2445.7, and 2447.8 cm^{-1}, respectively. The latter can be seen in more detail in Figure 8 which shows photoconductivity (left) and IR absorption (right) spectra recorded for the samples treated in D$_2$ (top) and H$_2$ + D$_2$ gas. Similar results were obtained for the LVMs of interstitial hydrogen, which are not presented here since the corresponding lines are significantly broader than those of deuterium.

Figure 8 reveals that qualitatively PC and IR absorption spectra are very similar which gives further support to the assignment of D$_g^0$ and D$_e^0$ (H$_g^0$ and H$_e^0$) modes to the neutral charge state of the deuterium (hydrogen) donor. Note that if both isotopes are simultaneously present in the sample, the shape of the resonances differs from that of pure deuterium. Similar to the case of hydrogen in ZnO, we explain this by the combined effect of a positive Fano resonance resulting from the deuterium donor and the reduction of photocurrent due to the hydrogen donor.

The photoconductivity spectra obtained for hydrogenated rutile samples lead us to the conclusion that the behavior of interstitial hydrogen in this oxide is similar to that of in ZnO. In both materials, LVMs of hydrogen appear as Fano resonances with $q \to +\infty$, which implies that hydrogen should be the main donor in the samples. This sets an upper limit of 300 meV for the ionization energy of hydrogen in rutile (see Fig. 1). The lowest frequency at which the photocurrent is detected in our setup occurs at around 1000 cm^{-1}, which should further reduce the ionization energy of the interstitial hydrogen to 120 meV.

This conclusion is not in line with first principles calculations predicting a small polaron rather than shallow-donor-like behavior of an electron bound to the hydrogen donor in rutile.[23,24] In order to explain the controversy between theory and electrical measurements revealing delocalized free

electron behavior, Janotti *et al.* proposed that there is an energy barrier that confines an electron to its delocalized, metastable state and keeps it from accessing the small polaron regime at helium temperatures.[38,39]

This model, however, does not explain the thin structure of the D^0 (H^0) modes associated by Bekisli *et al.* with a small polaron localized at three different nearby Ti sites around interstitial hydrogen.[33] Further theoretical and experimental investigations are necessary to solve the controversy about behavior of hydrogen in rutile TiO_2.

IV. SUMMARY

Hydrogen-related defects in ZnO and rutile TiO_2 were investigated by means of photoconductivity and IR absorption spectroscopy. It is shown that vibrational modes of interstitial hydrogen in both semiconductors can be detected as Fano resonances in photoconductivity spectra. Based on the frequency of the resonances, it is concluded that under experimental conditions employed in our study the apparent ionization energy of the interstitial hydrogen donor in rutile TiO_2 is less than 300 meV. It is demonstrated that photoelectric spectroscopy can directly reveal a type of electrical activity of defects resulting in local vibrational modes. Moreover, this method of detection of LVMs is shown to be preferential for the spectral regions inaccessible for the standard IR absorption spectroscopy and/or for semiconductor thin films.

ACKNOWLEDGMENTS

APPENDIX: LOCAL MODES AS FANO RESONANCES

The results presented here imply that conclusions about electrical activities of defects giving rise to the Fano resonances in the photoconductivity spectra due to the vibrational modes critically depend on the parameter q in Eq. (1). To get insight into the shape of the Fano resonances due to a local vibrational mode of an electrically active defect, we apply formalism proposed in Refs. 40 and 41.

First, we consider a simple system with two excited states coupled by a matrix element V (see Fig. 9). The unperturbed system has a ground state $|g\rangle$, an excited electronic state $|e\rangle$, and a LVM with the excited state $|p\rangle$. In photoconductivity spectra, only transitions between the ground state and the electronic state are detected with an operator $\hat{T}$.

The Hamiltonian of this system is

$$H = \begin{pmatrix} E_e & V \\ V & E_p \end{pmatrix}. \quad (A1)$$

Keeping in mind a problem of the electronic continuum, the Green's function operator can be introduced
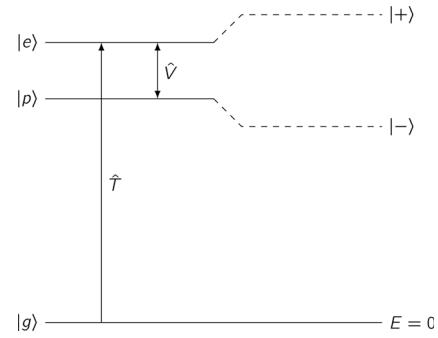

FIG. 9. System with an electronic $|e\rangle$ and vibronic $|p\rangle$ states coupled by a matrix element V.

$$G(z) = \frac{1}{(E_e - z)(E_p - z) - V^2} \begin{pmatrix} E_p - z & -V \\ -V & E_e - z \end{pmatrix}, \quad (A2)$$

with $z = E + i0^+$. The trace of G is invariant with respect to the basis functions

$$Tr(G) = \sum_k \langle k|(H - z)^{-1}|k\rangle = \sum_k \frac{1}{E_k - E - i0^+}. \quad (A3)$$

The photoconductivity spectrum due to Hamiltonian (A1) is given by

$$I(E) = \sum_{a=\pm} |\langle g|\hat{T}|a\rangle|^2 \delta(E_a - E). \quad (A4)$$

This expression can be rewritten as

$$I(E) = \langle g|\hat{T}\left(\sum_{a=\pm} |a\rangle\langle a|\delta(E_a - E)\right)\hat{T}|g\rangle. \quad (A5)$$

Expression in parenthesis can be represented as

$$\sum_{a=\pm} |a\rangle\langle a|\delta(E_a - E) = \frac{1}{\pi} Im \sum_{i,j=e,p} |i\rangle G(z)\langle j|. \quad (A6)$$

Since only the $|g\rangle \rightarrow |e\rangle$ transition is not equal to zero, from this expression, (A2), and (A5) we get

$$I(E) = \frac{1}{\pi} Im \frac{|\langle g|\hat{T}|e\rangle|^2 (E_p - z)}{(E_e - z)(E_p - z) - V^2}. \quad (A7)$$

We now come to the case of interaction of a sharp LVM level $|p\rangle$ with an electronic continuum. We assume that each level $|e\rangle$ in the continuum couples to the ground state with a constant matrix element $\langle g|\hat{T}|e\rangle$. In this case, Eq. (A7) can be also employed if we replace

$$E_e - z \rightarrow \frac{1}{g(z)}, \quad \text{where} \quad g(z) = \sum_e \frac{1}{E_e - z} \quad (A8)$$

is the unperturbed Green's function for the electronic continuum. The density of states is given by

$$\rho(E) = \frac{1}{\pi} Im[Tr(g)]. \quad (A9)$$

Its Hilbert transform is

$$R(E) = P \int \frac{\rho(E')}{E - E'} dE', \quad (A10)$$

where P stands for "principal value." With this modification Eq. (A7) becomes

$$I(E) = \frac{|\langle g|\hat{T}|e\rangle|^2 \rho(E)(E_p - E)^2}{\left[E_p - E + V^2 R(E)\right]^2 + \pi^2 V^4 \rho(E)^2}.$$

If we define

$$\epsilon = \frac{E - E_p - V^2 R(E)}{\pi V^2 \rho(E)} \quad \text{and} \quad q = \frac{R(E)}{\pi \rho(E)}, \quad (A11)$$

we get the Fano curves (cf. Eq. (1))

$$I(E) = \rho(\epsilon)|\langle g|\hat{T}|e\rangle|^2 \frac{(q + \epsilon)^2}{1 + \epsilon^2} \quad (A12)$$

with the linewidth Γ and the additional shift Ω

$$\hbar\Gamma/2 = \pi V^2 \rho(E), \quad \hbar\Omega = V^2 R(E). \quad (A13)$$

Interestingly, the shape of the Fano curve (parameter q in Eq. (A11)) turns out to be independent of the coupling V between vibrational and electronic excitations and is determined solely by the properties of the host crystal. It follows from here that if the donor/acceptor of interest dominates the sample, the shape of the Fano resonances due to its LVMs can be obtained *a priori* from the first principles theory. The corresponding calculations are called for to verify this conclusion.

[1]*Identification of Defects in Semiconductors*, Semiconductors and Semimetals Vol. 51B, edited by M. Stavola (Academic Press, San Diego, 1999).

[2]S. J. Pearton, J. W. Corbett, and M. Stavola, *Hydrogen in Crystalline Semiconductors* (Springer-Verlag, Berlin, 1992).

[3]S. G. Koch, E. V. Lavrov, and J. Weber, Phys. Rev. Lett. **108**, 165501 (2012).

[4]A. Janotti and C. G. Van de Walle, Nat. Mater. **6**, 44 (2007).

[5]S. M. Kogan and T. M. Lifshits, Phys. Status Solidi A **39**, 11 (1977).

[6]U. Fano, Phys. Rev. **124**, 1866 (1961).

[7]E. V. Lavrov, F. Herklotz, and J. Weber, Semicond. Sci. Technol. **30**, 024004 (2015).

[8]E. V. Lavrov, J. Weber, F. Börrnert, C. G. Van de Walle, and R. Helbig, Phys. Rev. B **66**, 165205 (2002).

[9]F. Herklotz, E. V. Lavrov, and J. Weber, Phys. Rev. B **83**, 235202 (2011).

[10]R. Helbig, J. Cryst. Growth **15**, 25 (1972).

[11]C. G. Van de Walle, Phys. Rev. Lett. **85**, 1012 (2000).

[12]E. V. Lavrov, F. Herklotz, and J. Weber, Phys. Rev. B **79**, 165210 (2009).

[13]D. G. Thomas and J. J. Lander, J. Chem. Phys. **25**, 1136 (1956).

[14]E. V. Lavrov, J. Weber, and F. Börrnert, Phys. Rev. B **77**, 155209 (2008).

[15]F. Herklotz, K. M. Johansen, A. Galeckas, T. N. Sky, and B. G. Svensson, Phys. Status Solidi B **253**, 273 (2016).

[16]M. G. Wardle, J. P. Goss, and P. R. Briddon, Phys. Rev. B **72**, 155108 (2005).

[17]S. F. J. Cox, J. S. Lord, S. P. Cottrell, J. M. Gil, H. V. Alberto, A. Keren, D. Prabhakaran, R. Scheuermann, and A. Stoykov, J. Phys.: Condens. Matter **18**, 1061 (2006).

[18]K. Xiong, J. Robertson, and S. J. Clark, J. Appl. Phys. **102**, 083710 (2007).

[19]H. Li and J. Robertson, J. Appl. Phys. **115**, 203708 (2014).

[20]H. Tang, K. Prasad, R. Sanjinés, P. E. Schmid, and F. Lévy, J. Appl. Phys. **75**, 2042 (1994).

[21]H. Tang, F. Lévy, H. Berger, and P. E. Schmid, Phys. Rev. B **52**, 7771 (1995).

[22]M. Dou and C. Persson, J. Appl. Phys. **113**, 083703 (2013).

[23]F. Filippone, G. Mattioli, P. Alippi, and A. A. Bonapasta, Phys. Rev. B **80**, 245203 (2009).

[24]P. Deák, B. Aradi, and T. Frauenheim, Phys. Rev. B **83**, 155207 (2011).

[25]M. Setvin, C. Franchini, X. Hao, M. Schmid, A. Janotti, M. Kaltak, C. G. Van de Walle, G. Kresse, and U. Diebold, Phys. Rev. Lett. **113**, 086402 (2014).

[26]E. V. Lavrov, Phys. Status Solidi A **212**, 1494 (2015).

[27]E. V. Lavrov, Phys. Rev. B **93**, 045204 (2016).

[28]R. J. Swope, J. R. Smyth, and A. C. Larson, Am. Mineral. **80**, 448 (1995).

[29]M. V. Koudriachova, S. W. de Leeuw, and N. M. Harrison, Phys. Rev. B **70**, 165421 (2004).

[30]E. J. Spahr, L. Wen, M. Stavola, L. A. Boatner, L. C. Feldman, N. H. Tolk, and G. Lüpke, Phys. Rev. Lett. **104**, 205901 (2010).

[31]K. Shimomura, R. Kadono, A. Koda, K. Nishiyama, and M. Mihara, Phys. Rev. B **92**, 075203 (2015).

[32]A. T. Brant, S. Yang, N. C. Giles, and L. E. Halliburton, J. Appl. Phys. **110**, 053714 (2011).

[33]F. Bekisli, W. B. Fowler, and M. Stavola, Phys. Rev. B **86**, 155208 (2012).

[34]D. A. Panayotov and J. T. Yates, Jr., Chem. Phys. Lett. **436**, 204 (2007).

[35]S. Yang, A. T. Brant, N. C. Giles, and L. E. Halliburton, Phys. Rev. B **87**, 125201 (2013).

[36]H. Sezen, M. Buchholz, A. Nefedov, C. Natzeck, S. Heissler, C. Di Valentin, and C. Wöll, Sci. Rep. **4**, 3808 (2014).

[37]R. C. Vilão, R. B. L. Vieira, H. V. Alberto, J. M. Gil, A. Weidinger, R. L. Lichti, B. B. Baker, P. W. Mengyan, and J. S. Lord, Phys. Rev. B **92**, 081202 (2015).

[38]E. Yagi, R. R. Hasiguti, and M. Aono, Phys. Rev. B **54**, 7945 (1996).

[39]A. Janotti, C. Franchini, J. B. Varley, G. Kresse, and C. G. Van de Walle, Phys. Status Solidi RRL **7**, 199 (2013).

[40]M. Lannoo and J. Bourgoin, *Point Defects in Semiconductors I* (Springer-Verlag, Berlin, Heidelberg, New York, 1981).

[41]*Light Scattering in Solids I*, Topics in Applied Physics Vol. 8, edited by M. Cardona (Springer, Berlin, 1983).